



## Carbon Surfaces Doped with (Co<sub>3</sub>O<sub>4</sub>-Cr<sub>2</sub>O<sub>3</sub>) Nanocomposite for High-Temperature Photo Thermal Solar Energy Conversion Via Spectrally Selective Surfaces

R. N. Abed<sup>\*1</sup>, A. R. N. Abed<sup>1</sup>, E. Yousif<sup>2</sup>

<sup>1</sup> Mechanical Engineering Department, Engineering College, Al-Nahrain University, P.O. Box: 64040, Jadriah, Baghdad, Iraq.

<sup>2</sup> Department of Chemistry, College of Science, Al-Nahrain University, P.O. Box: 64040, Jadriah, Baghdad, Iraq.

### ARTICLE INFO

Article history:

Received: 10 Nov 2020

Final Revised: 30 Jan 2021

Accepted: 01 Feb 2021

Available online: 22 Feb 2021

Keywords:

Cobalt oxide

Chromium oxide

Optical properties

Energy band gap

Absorptivity.

### ABSTRACT

*Invention new thin films nano-coating to obtain high-level performance spectrally selective surfaces to enhance solar energy by spin and casting methods, thin films coating are deposited by these techniques on aluminum and glass substrates that were pre-cleaned. Nanocomposite thin film coating comprising (Co<sub>3</sub>O<sub>4</sub>:Cr<sub>2</sub>O<sub>3</sub>) and carbon to gain an economical coating. The coating has a high absorptivity of solar energy. Nanomaterials have been used in various concentration ratios to dope carbon, and Energy Dispersive Analysis (EDX) was used to determine carbon ash's chemical composition; SEM measured its practical size. Optical properties have been studied by the UV-Visible Spectra and reflectivity tests in a range from 250-1300 nm at room temperature. Absorbance coefficient, transmittance, reflectance, skin depth, optical density, optical energy gap (Eg), and Urbach energy of nanocomposite thin films have also been specified. The Eg of doped C has been measured with different concentration ratios of (Co<sub>3</sub>O<sub>4</sub>:Cr<sub>2</sub>O<sub>3</sub>) such as sample F (0.5:2.5/7), sample G (1:2/7), sample H (1.5:1.5/7), the sample I (2:1/7), and sample K (2.5:0.5/7) wt. %, the concentration of C is fixed for all samples (7) wt. %. The results revealed that the Eg is ranged (2.9-3.9 eV) and the absorptivity in the ranged (88-93.2 %) for all doped samples. The absorptivity values of nanocomposites are very close to semiconductor elements, which have high absorptivity to the wavelength intensity. The synthesized coating will be used over a flat plate collector as a trap to absorb solar energy for a highly feasible selective surface. Prog. Color Colorants Coat. 14 (2021), 301-315 © Institute for Color Science and Technology.*

### 1. Introduction

Solar energy is one of the primary energy sources of the earth has a high electromagnetic wavelength. Herein is suggested a possible coating by designing nanocomposite thin film, which absorbs the maximum amount of incident solar radiation. In Iraq, most regions have strong sunlight, around 300 days in a year

[1]. The amount of solar energy per square meter in a day can be about 5 kWh [1]. The technology to produce nanocomposite thin films is used to absorb solar energy and utilizing coating on the flat plate collector to harness this solar energy. This energy can be achieved in homes for domestic application heating the water or ventilation, and residential houses. The

\*Corresponding author: \* [rasheed.n.abed@ced.nahrainuniv.edu.iq](mailto:rasheed.n.abed@ced.nahrainuniv.edu.iq)  
[rasheednema@yahoo.com](mailto:rasheednema@yahoo.com)

absorbed energy of coating on the flat plate collector surface was acquired to be a spectrally selective surface. This surface has low emission and high absorption solar energy; after then, solar energy is converted to water heating for domestic applications [1, 2]. Doping nanomaterials to carbon may produce a remarkable change in its properties with doping [3, 4]. Therefore, optical properties are most important for many applications, such as coating flat plate collectors, microelectronic, and optoelectronic devices depending on the properties of reflectance and absorbance for nanocomposite thin films during their preparation [5].

Cobalt oxide ( $\text{Co}_3\text{O}_4$ ) is a prevalent factor with several oxidization states because of its unusual chemical and physical features.  $\text{Co}_3\text{O}_4$  is utilized exceptionally in ceramics production as a further element to produce blue coloring glazes. Its compounds may be used in photo-catalysis [6-10] and absorbance energy storage [5, 12]. Furthermore, cobalt oxide does have significant electric properties, after added  $\text{Co}_3\text{O}_4$  to a chromium oxide is created a porous conductive network [11-15].  $\text{Co}_3\text{O}_4$  is multilateral oxide sided between the oxides family, it has properties similar to a p-type semiconductor, and the band gap is ranged among (2.23–3.38 eV) [16, 18].  $\text{Co}_3\text{O}_4$  has attracted exceptional attention in field application technology of pigments and solar selective surfaces [17-21]. Nanoparticle and micro size of  $\text{Co}_3\text{O}_4$  supplied perfect performance of electrochemical in different field implementations such as electronic applications and flat plate surface coating [20-24]. Nanocrystalline thin films were deposited on steel and glass substrates, which constitute nickel-cobalt oxides ( $\text{NiO-CoO}$ ) to produce thin films of various concentrations using a chemical bath method deposition (CBD). The thin films exhibited semiconductor features, demonstrated super capacitive demeanor, and had bandgap energy ranging among (2.75-2.95 eV) [25-26]. Further, ZnO doped with cobalt (Co) by ultra-high vacuum (UHV) to create a new structure of Co/ZnO was performed by a chemical bath deposition method, and this Nanocomposite was used in electronic sensor [27-28]. On the other hand, manganese (Mn) doped cobalt oxide  $\text{Co}_3\text{O}_4$  to produce unique network porous by a hydrothermal process, which used electrode in super-capacitors, and the composite  $\text{Co}_3\text{O}_4/\text{Mn}$  was annealed in atmosphere air with further processes [29]. Then, titanium oxide ( $\text{TiO}_2$ ) doped cobalt (Co) to fabricate a composite by a

spin coating process. The composite was promised window to advance the performance of the solar cell and the composite has a band gap about (4.04 eV) [30, 31].

Chromium oxide ( $\text{Cr}_2\text{O}_3$ ) has semiconductor property, its direct and indirect band gaps are ranged about (3.00-3.40 eV). Its properties have a high melting point, p-type semiconductor, superior resistance for corrosion and electrical conductivity in high-temperature [32, 33]; from these special features, chromium oxide was earned many applications in the equipment of solar photovoltaic, pigments, nanocomposite coating, and photo-catalytic [34-38]. Chromium oxide thin film was prepared by a sol-gel process. It is deposited on a substrate of glass; this substrate was heated to 50 °C and annealed to 200 °C by an oven microwave to get a high crystalline structure of Nanocomposite [38-40]. Indeed, composite thin film ( $\text{Cr}_2\text{O}_3:\text{CuO}$ ) was synthesized from an equal concentration of these nanomaterials in the sputtering magnetron method and deposited on a substrate of quartz, and a thin film is utilized in a gas sensing device [41-43]. Moreover, thin films composite ( $\text{Cr}_2\text{O}_3:\text{PVC}$ ) was constituted chromium oxide and polyvinyl chloride (PVA). Nanoparticles ( $\text{Cr}_2\text{O}_3$ ) doped polyvinyl chloride (PVA), and composite thin film energy gap declines with increase nano concentration and optical properties of PVA are affected with adding  $\text{Cr}_2\text{O}_3$  [44]. Moreover, selective solar absorber coating consists of multilayer  $\text{Cr}_2\text{O}_3/\text{Cr}/\text{Cr}_2\text{O}_3$  has been deposited on a substrate of stainless steel by utilizing vacuum evaporative electron beam. The optical study for these selective surfaces in multilayer coating thin films was demonstrated higher absorptivity coefficient ( $\alpha = 0.89$ ) and decline the emissivity to ( $\epsilon = 0.15$ ) at temperature 300 °C, when the sample is annealed at a temperature 400 °C in 24 h. From the theoretical computation by using CODE software, the value of absorptivity coefficient is increased through it ( $\alpha = 0.916$ ) and the emissivity still invariant at the same value ( $\epsilon = 0.15$ ) [41, 45]. In addition, the composite ( $\text{Cr}_2\text{O}_3:\text{TiO}_2$ ) is composed of nano-powder titanium oxide with variable concentration of  $\text{Cr}_2\text{O}_3$  to synthesis coating with a high-temperature solid-state process. A nanoparticle of chromium oxide ( $\text{Cr}_2\text{O}_3$ ) was used to dope  $\text{TiO}_2$  with created coating was deposited on the substrate by plasma spraying method and the coating thickness became (1.9 mm) at 5% content from  $\text{Cr}_2\text{O}_3$ , where it is used in solar energy capturing [46, 47].

In brief, this paper discusses synthesis unique thermally nanocomposite thin films, which are fabricated from cobalt oxide and chromium oxide to dope carbon (fuel ash) (Co<sub>3</sub>O<sub>4</sub>:Cr<sub>2</sub>O<sub>3</sub>/C). The nanocomposite thin films capable to absorb solar energy have been synthesized from solids component nanomaterials Co<sub>3</sub>O<sub>4</sub> and Cr<sub>2</sub>O<sub>3</sub>, which mixed with molasses and deionized water by spin and casting methods. To the best of our knowledge, there is no study on the optical properties of this coating was published until now. The characterization of thin films (Co<sub>3</sub>O<sub>4</sub>:Cr<sub>2</sub>O<sub>3</sub>/C) was obtained by UV-Visible and reflectivity equipment to compute optical properties and produce attractive band gap for carbon. Also, in this paper is discussed surface morphology and optical properties of spin coating, with deposit nanocomposite thin films (Co<sub>3</sub>O<sub>4</sub>:Cr<sub>2</sub>O<sub>3</sub>/C) on glass and aluminum substrates. In addition, Urbach and band gap energy have been discussed.

## 2. Experimental

Spin and casting methods were used to produce thin films of nanocomposite materials that precipitated on

the aluminum (Al) and glass substrates. Carbon ash has been brought from Doura Refinery as an output of the combustion. it was used after some process carried out, such as sieving to remove all lingering stuff. The nanomaterials Co<sub>3</sub>O<sub>4</sub> and Cr<sub>2</sub>O<sub>3</sub> were equipped by Changsha Easchem company /Hunan China, with average particle size of 20 nm and 99.9 % purity, the materials utilized in the research with their purity and particle size listed in the Table 1.

The SEM examination was used to determine the particles size of carbon ash, which was found in range from (29.62-93.22 μm) and the EDS examination Figure 1 shown the chemical composition of carbon.

AFM analysis was used to be ascertain that the particle size of the Co<sub>3</sub>O<sub>4</sub> and Cr<sub>2</sub>O<sub>3</sub> in nano scale as shown in Figure 2.

### 2.1. Preparation of Nanocomposite materials

The materials such as carbon fuel ash powdered and high purity nanomaterials (Co<sub>3</sub>O<sub>4</sub>:Cr<sub>2</sub>O<sub>3</sub>) have been chosen in appropriate proportions, their mass ratios were weighted by electronic balance with 5 digits, which used to get the desired amount of compositions.

**Table 1:** materials have been utilized in the research.

No.	Materials	Purity %	Suppliers	Particle size
1	Carbon ash	Raw after sieving	Doura Refinery	29.62-93.22 (μm)
2	Co <sub>3</sub> O <sub>4</sub> nano	99.9	Changsha Easchem /Hunan China	20 (nm)
3	Cr <sub>2</sub> O <sub>3</sub> nano	99.9	Changsha Easchem /Hunan China	20 (nm)

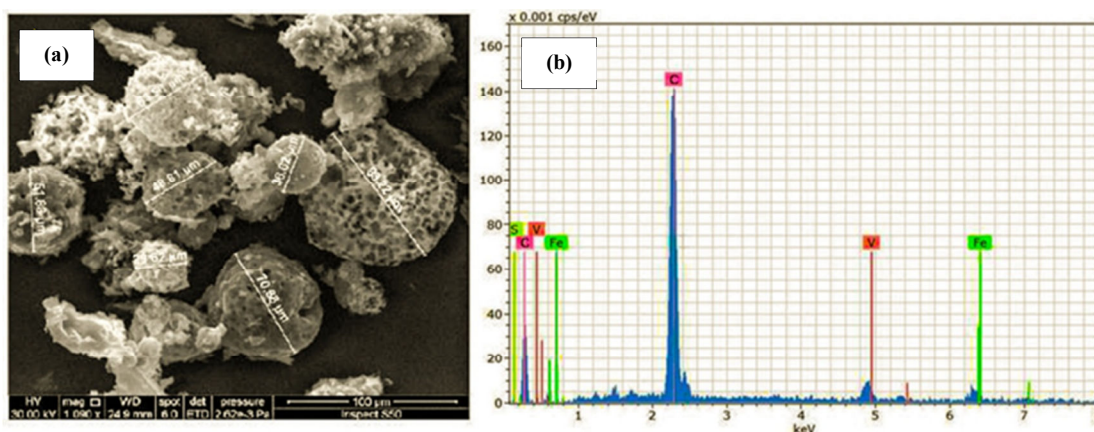


**Figure 1:** (a) shows the SEM photograph of carbon ash, (b) EDS analysis of carbon ash particles.

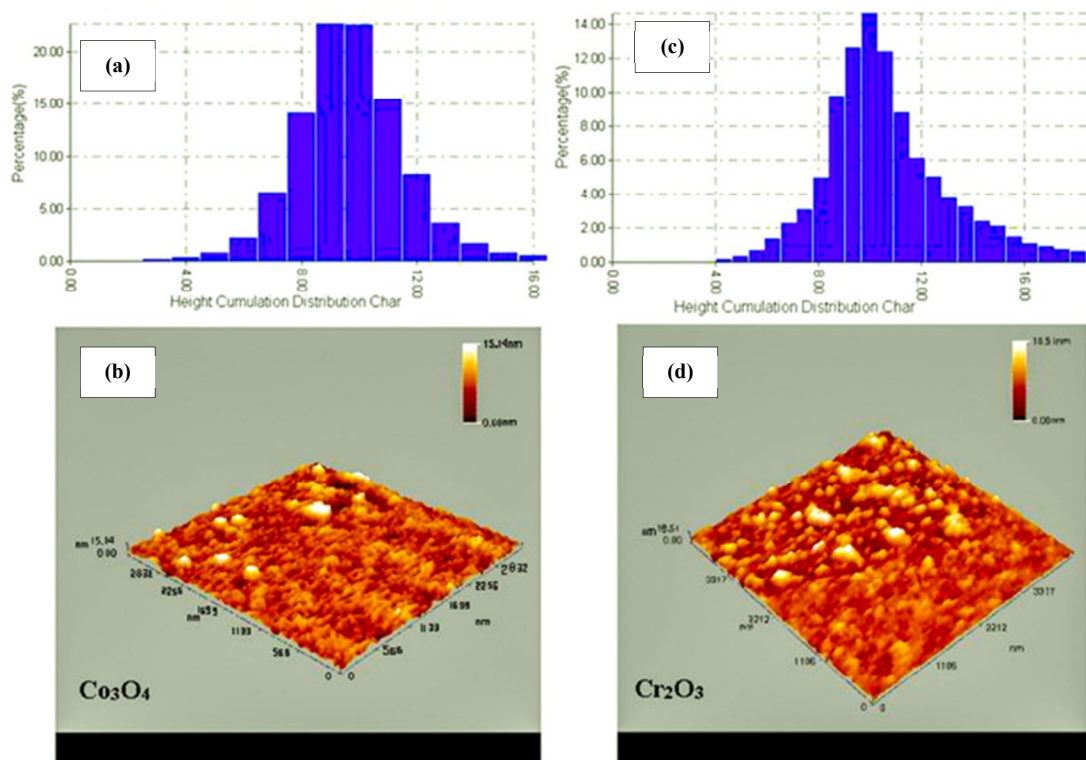


**Figure 2:** (a) accumulation distribution of  $\text{Co}_3\text{O}_4$  nanoparticles, (b) AFM 3D examination of  $\text{Co}_3\text{O}_4$ , (c) accumulation distribution of  $\text{Cr}_2\text{O}_3$  nanoparticles, and (d) AFM examination of  $\text{Cr}_2\text{O}_3$  accumulation distribution.

The percentage of carbon content is 7 wt. %, which added to the high purity ( $\text{Co}_3\text{O}_4:\text{Cr}_2\text{O}_3$ ) with different concentration. Sample F (0.5:2.5/7), sample G (1:2/7), sample H (1.5:1.5/7), sample I (2:1/7), and sample K (2.5:0.5/7) wt.% to form the colloidal for a homogenous mixture are as illustrated in the Table 2.

The stirrer process was used for 3 hours to stir the solid components with deionized water and molasses to achieve very well mixing. The colloidal solution was placed in a glass tube followed by vigorous mixing; the nanocomposite thin films were deposited on pre-cleaned Al and glass substrates. The dimensions of the

substrate ( $2.5 \times 5 \text{ cm}^2$ ), these substrates were completely cleaned several times by using a detergent solution such as ethanol and acetone to remove any degrease on them. Finally, the samples rinsed in deionized water and dried in the oven at ( $60 \text{ }^\circ\text{C}$ ) for 1 h. The nanocomposite materials were deposited on substrates by spin coating and casting method and dried in the oven at ( $90 \text{ }^\circ\text{C}$ ) to remove any residual solution in samples. The thickness of nanocomposite thin films was measured around 300 nm by using an SEM device.

**Table 2:** compositions of samples of nanomaterials and carbon in weight %.

No.	Sample	Nanomaterial content wt. % ( $\text{Co}_3\text{O}_4:\text{Cr}_2\text{O}_3$ )	Carbon content wt. %
1	F	0.5:2.5	7
2	G	1.0:2.0	7
3	H	1.5:1.5	7
4	I	2.0:1.0	7
5	K	2.5:0.5	7

## 2.2. Characterization of the thin films

All the specimens were prepared and analyzed by using diffusion reflectance wavelength, (Avantes DH-S-BAL-2048, UV-Visible Spectro-2048), which are recorded results with wavelength range from (250-1300 nm), with wavelength step 2 nm. Then by using computerized SHIMADZU, UV-VISIBLE SPECTROMETER UV-1650 PC, the absorption spectra were recorded in the wavelength range from (200-800 nm), with wavelength step 2 nm also. All tests of optical properties were achieved at room temperature (27 °C).

## 3. Results and Discussion

### 3.1. Optical properties of thin films

The optical properties of thin films (Co<sub>3</sub>O<sub>4</sub>:Cr<sub>2</sub>O<sub>3</sub>/C nanocomposite) plays a significant role in understanding the nature of optoelectronic Properties. The properties of nanocomposite thin films are interpreted in the standpoint of interference between incident solar radiation of semiconducting thin films, and through the study of band gap energy gained from optical absorption to demonstrate the band structure of semiconductors [48, 49]. The investigation and discussion of optical nanocomposite thin films (Co<sub>3</sub>O<sub>4</sub>:Cr<sub>2</sub>O<sub>3</sub>/C) depend on measurements of reflectance,  $R(\lambda)$ , in the spectral range 250-1300 nm. These optical studies were utilized to determine the optical energy gap ( $E_g$ ) for nanocomposite thin films.

#### 3.1.1. Reflectance test results

The reflectivity wavelength  $R(\lambda)$ , of examined thin films nanocomposite (Co<sub>3</sub>O<sub>4</sub>:Cr<sub>2</sub>O<sub>3</sub>/C) samples (F, G, H, I, and K) are shown in Figure 3. Figure 3 cleared the spectra could be divided into two special regions: high absorption region of wavelength  $\leq 420$  nm and the absorption region lies between (420-800 nm). In the visible region between (420-800 nm), there is a good absorption of wavelength radiation and became invariant along the wavelength axis. Furthermore, the samples of (Co<sub>3</sub>O<sub>4</sub>:Cr<sub>2</sub>O<sub>3</sub>/C) has a high absorption nature and were exhibited in Figure 3 for all constitutes of thin film concentration. In addition, the absorption edge is shifted toward lower energies as the percentage of (Co<sub>3</sub>O<sub>4</sub>:Cr<sub>2</sub>O<sub>3</sub>) increases [50, 51]. This confirms that incident light on nanocomposite thin films thoroughly absorbed, which provide good evidence that surfaces of deposited thin films have roughness nature to absorb the incident light in the visible region and near I.R.

Therefore, the absorptivity ( $\alpha$ ) can be computed from the relation between reflectivity ( $R$ ) and absorptivity ( $\alpha$ ), for all thin films, absorptivity ( $\alpha$ ) values are ranged between (88-92 %) [52]. All samples have a low value of reflectance; this means that samples don't permit wavelength to reflect through the thin film to give high absorptivity. From these data, optical absorption for samples is increased when reflectance and transmittance be a lower value. The surfaces of deposited thin films for Nanocomposite on substrates has roughness nature to harness the incident light in visible and near IR. This confirms that incident light on nanocomposite films thoroughly absorbed. Additionally, thin films obtained for all samples are proved to be a semiconductor.

#### 3.1.2. Calculation of absorbance coefficient

The optical features of materials depend on many variables such as the precursory conditions, the morphology of surface, and preparation mechanism, according to their interaction and doping by other materials with it. The examination of the spectral demeanor of absorption coefficient for any semiconducting material provides more instruction around electronic levels in the part of high energy for optical absorption spectrum, whilst the other part of lower energy coincides with vibrations of atoms [52, 53]. Different implementations are depended on the optical absorption spectrum of Nanocomposite (Co<sub>3</sub>O<sub>4</sub>:Cr<sub>2</sub>O<sub>3</sub>/C), the absorption coefficient may be determined from the measurement of absorbance values with wavelength and computes from the Beer lambert's law [54, 55]:

$$\ln \frac{I}{I_0} = e^{-\alpha t}, \alpha = 2.303 \times \frac{A}{t} \quad (1)$$

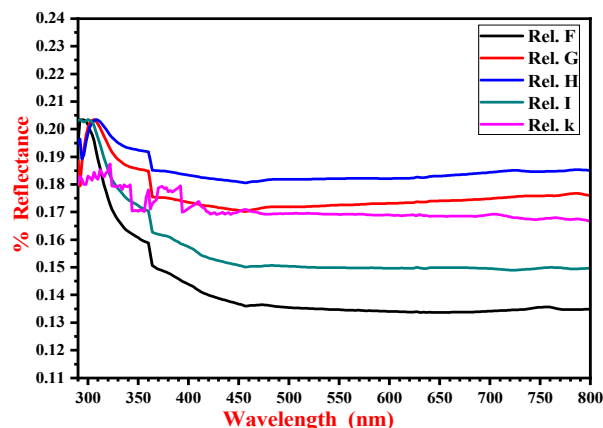


Figure 3: reflectance test with the wavelength for all samples.

Where, ( $\alpha$ ) is the absorption coefficient in ( $\text{cm}^{-1}$ ), ( $A$ ) is the absorbance value, ( $t$ ) is the thickness in (cm). The absorption coefficient of nanocomposite thin films ( $\text{Co}_3\text{O}_4:\text{Cr}_2\text{O}_3/\text{C}$ ) with their contents ( $0.05:2.5 \leq x \leq 2.5:0.05$  at. %) is dependent on wavelength as shown in Figure 4. The results in the figure shown that the absorption coefficient value of ( $\alpha$ ) declines with increment in wavelength for all samples of Nanocomposite ( $\text{Co}_3\text{O}_4:\text{Cr}_2\text{O}_3/\text{C}$ ) until a certain wavelength ( $\lambda=370$  nm), after that, the absorption coefficient ( $\alpha$ ) nearly invariant along the axis of wavelength. In Figure 4 is exhibited the concentration of sample K (2.5:0.5/7 wt. %) has the best concentration and have high absorbance coefficient; the high absorbance value is attributed to the content of ( $\text{Co}_3\text{O}_4$ ) in the mixture K as shown in Table 2.

The absorption edge in each composition was determined by extrapolating the absorption coefficient curve to interrupt the wavelength line at a specified point. The location of intersection for the point gives the optical band edge amount. It was noticed that the intersection points located in the UV-Visible zone range (300-400 nm) for all thin films and the absorption edge were observed in Figure 5. It was observed that the absorption edge and the wavelength was increased with increasing the  $\text{Co}_3\text{O}_4/\text{Cr}_2\text{O}_3$  ratio. In nanocomposite thin films, the absorption edge value was listed in Table 3 for the Nanocomposite ( $\text{Co}_3\text{O}_4:\text{Cr}_2\text{O}_3/\text{C}$ ). This shifting is prospective demeanor, which indicates increasing the ratio of ( $\text{Co}_3\text{O}_4$ ) element in Nanocomposite and will decrease the optical band gap [54, 56].

Further, the optical density ( $D_{opt}$ ) is proportional to both concentrations and thin film thickness of samples and depending on absorption for the coated layer.  $D_{opt}$  of present nanocomposite thin films ( $\text{Co}_3\text{O}_4:\text{Cr}_2\text{O}_3/\text{C}$ ) can be determined by utilizing this equation (Eq. 2) [54]:

$$D_{opt} = \alpha t \quad (2)$$

Where, ( $\alpha$ ) is the absorbance ( $\text{cm}^{-1}$ ), ( $t$ ) is the film thickness (cm).

In Figure 6 interprets the variance of optical density with photon energy. The variation of optical density is noticed with photon energy and is alike to the demeanor of the absorbance coefficient but opposite, where optical density increased with increased content of ( $\text{Co}_3\text{O}_4$ ) in all mixtures for thin films with a wavelength of all samples. From Figure 6 has been determin specimen K with concentration of (2.5:0.5/7 wt. %) as the best concentration with high optical density dependent on the absorption coefficient, this is attributed to increase in the content of ( $\text{Co}_3\text{O}_4$ ).

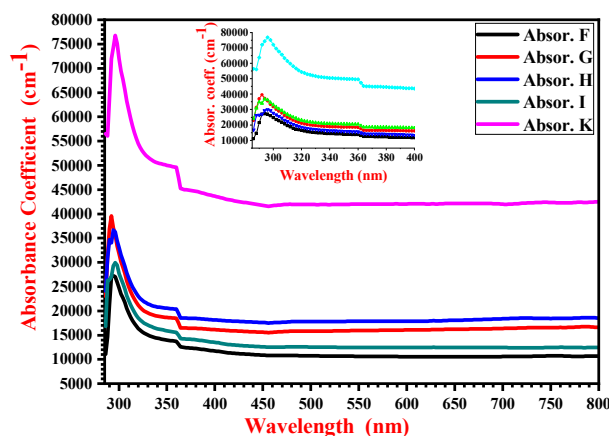


Figure 4: absorption coefficient variation with the wavelength for all samples.

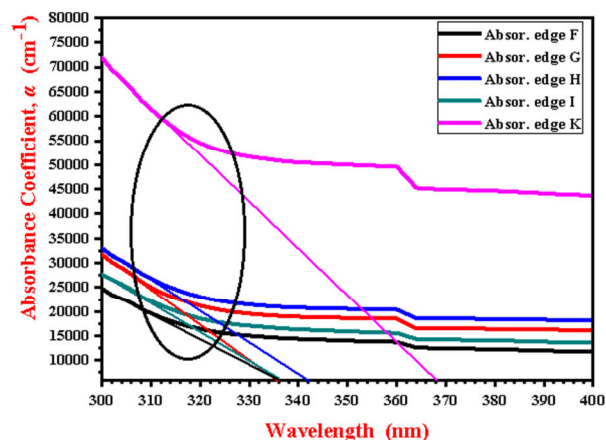
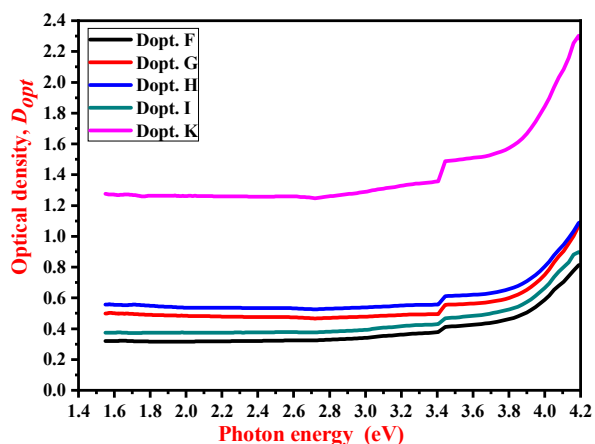


Figure 5: absorption coefficient edge shifted with increase  $\text{Co}_3\text{O}_4$  ratio.

Table 3: absorption edge value for all samples.

Absorption edge Sample F (nm)	Absorption edge Sample G (nm)	Absorption edge Sample H (nm)	Absorption edge Sample I (nm)	Absorption edge Sample K (nm)
336	336	342	336	368



**Figure 6:** optical density of the Nanocomposite with the photon energy for all samples.

### 3.1.3. Skin depth for thin films

The electromagnetic wave inside thin films for the spectrum is dependent upon absorption of thin film, also there are many factors influence it: such as thickness, the ratio of doping material and extinction coefficient of thin films. Any material as a semiconductor has absorbed a portion of incident energy that enters sample and the remaining portion from this energy is reflected from a surface. Thus, there are several important factors related to photon absorption inside the texture of the thin film, as a skin depth and optical conductivity of nanocomposite thin films [55, 57]. Skin depth is dependent on photons vibration of particles and conductivity of thin films also, because the semiconductor conductivity depends toughly on band gap. In semiconductors, there is a relationship between the skin depth and optical features. The wavelength ( $\lambda$ ) as expressed in equation (3) [58]:

$$x = \frac{\lambda}{2\pi k} \quad (3)$$

Where, ( $x$ ) is the skin depth in (nm), ( $\lambda$ ) is the wavelength in (nm), ( $k$ ) is the extinction factor.

By utilizing the wavelength with extinction factor data, the skin depth can be calculated for nanocomposite thin films. Figure 7 shows skin depth is dependent on photon energy for thin films of Nanocomposite (Co<sub>3</sub>O<sub>4</sub>:Cr<sub>2</sub>O<sub>3</sub>/C). It is evident from the Figure 7, that skin depth ( $x$ ) is increased when increasing the photon energy and it is depended on the composition of (Co<sub>3</sub>O<sub>4</sub>:Cr<sub>2</sub>O<sub>3</sub>) in dopant carbon (C). The skin depth value is varied with increased photon energy along the axis of photon energy, until the value of photon energy is ( $h\nu=5.5$  eV), the skin depth is increased due to

concentration of samples G (1:2/7 wt. %) and K (2.5:0.5/7 wt. %) to a high values, this attributed to the content of (Cr<sub>2</sub>O<sub>3</sub>) in concentration G and to the content of (Co<sub>3</sub>O<sub>4</sub>) in concentration K, and then the skin depth decreases to the primary value. The increases in concentrations of (Co<sub>3</sub>O<sub>4</sub>:Cr<sub>2</sub>O<sub>3</sub>) leads to the darkness of thin films. This will lead to a reduction in the transparency amount for thin films. The curves that gained from data of skin depth-photon energy show the peaks in one region (5.5 eV) for the concentration G and K [55, 58].

### 3.1.4. Transmittance for the thin films

The optical transmission spectra of doped carbon (C) thin films with various concentrations of nano (Co<sub>3</sub>O<sub>4</sub>:Cr<sub>2</sub>O<sub>3</sub>) is shown in Figure 8. The transmittance intensity is increased by increasing wavelength. The transmittance is increased, when the concentration of nanomaterials (Co<sub>3</sub>O<sub>4</sub>:Cr<sub>2</sub>O<sub>3</sub>) to dope C increases. In Figure 8 the transmittance is started from the low value at the UV-Visible range until the value of wavelength ( $\lambda=370$ ) and increased in the visible range, then when wavelength increased and becomes invariant along wavelength axis. Further, the concentration of sample K (2.5:0.5/7 wt. %) is the best content for Nanocomposite (Co<sub>3</sub>O<sub>4</sub>:Cr<sub>2</sub>O<sub>3</sub>/C) has a lower value of transmittance [54, 58]. From these data, the optical absorption for samples is increased when transmittance is a lower value.

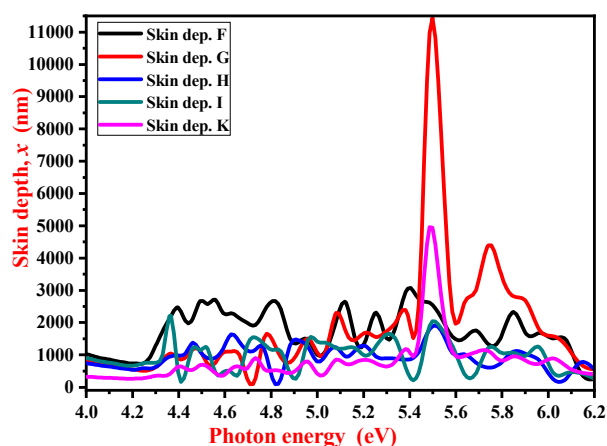


**Figure 7:** skin depth variation with photon energy for the nanocomposite thin films.

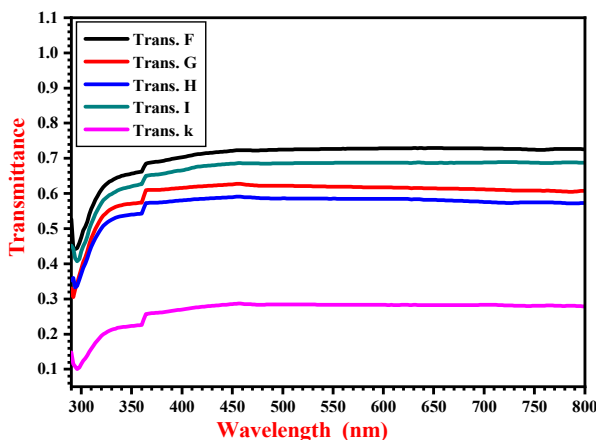


Figure 8: transmittance with the wavelength for all samples.

The surfaces of deposited thin films for Nanocomposite on substrates has a rough nature to harness the incident light in visible and near IR. This confirms that incident light on the nanocomposite films thoroughly absorbed. Additionally, thin films obtained for all samples were proved to be a semiconductor.

### 3.1.5. Refractive index and extinction factor

A base nanocomposite optical feature is a refractive index ( $n$ ), which is correlated directly to their optical features [54]. Refractive index was computed from the values of reflectance and extinction factor of nanocomposite thin films by utilizing this equation (Eq. 4):

$$n = \left[ \frac{1+R}{1-R} \right] + \sqrt{\frac{4R}{(1-R)^2} - k^2} \tag{4}$$

Where, ( $n$ ) is the refractive index, ( $R$ ) is the reflectivity and ( $k$ ) is the extinction factor.

The range of wavelengths for the refractive index is analyzed of the doped thin films as shown in Figure 9. All concentrations for the samples are indicated that the refractive index decreases with increasing wavelength along the x-axis for samples (F, G, H, I, and K) until the wavelength ( $\lambda=460$  nm), after this value the refractive index is invariant with wavelength increases along the axis.

The refractive index demeanor in Figure 9 was attributed to an increase in nano-materials content ( $\text{Co}_3\text{O}_4:\text{Cr}_2\text{O}_3$ ) in the Nanocomposite is lead to the increase of the packaging bulk as a result of filler amount for thin films.

The extinction factor ( $k$ ) for the doped samples are

depended on the wavelength range test and shown in Figure 10. The extinction coefficient is increased and its value decreases until the wavelength value ( $\lambda=370$  nm) for the nanocomposite thin films, whilst its value increased for all samples along the wavelength axis, the concentration of sample K (2.5:0.5/7 wt. %) has high extinction factor is attributed to the content of ( $\text{Co}_3\text{O}_4$ ) [55].

The extinction coefficient depended on the wavelength and the absorption coefficient, and then maybe computed through this equation (Eq. 5) [60, 61]:

$$k = \frac{\alpha \lambda}{4\pi} \tag{5}$$

Where, ( $\alpha$ ) the absorbance coefficient in ( $\text{cm}^{-1}$ ), ( $\lambda$ ) is the wavelength in (nm).

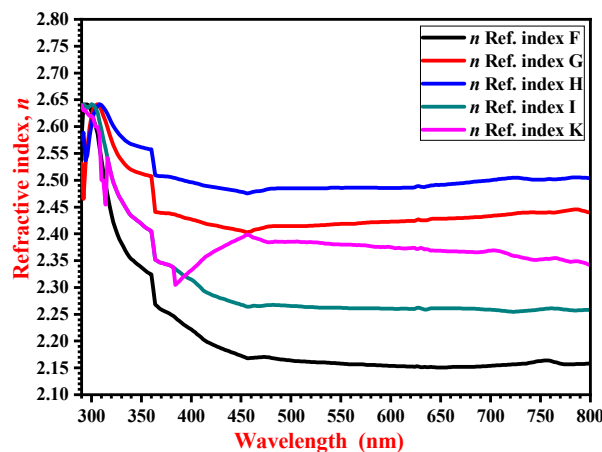


Figure 9: refractive index with the wavelength for the thin films.

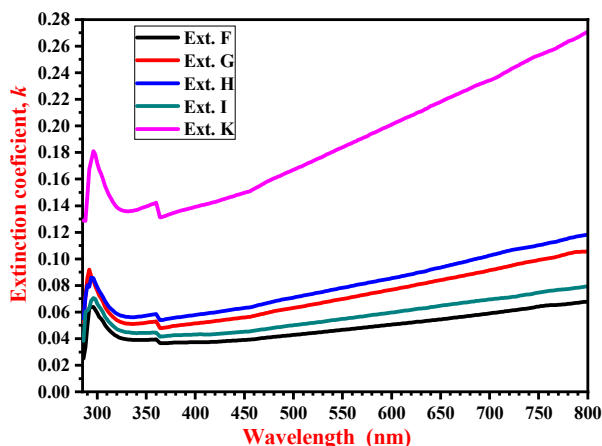


Figure 10: extinction coefficient with wavelength for all samples.

### 3.1.6. Real and imaginary of dielectric constant

The dielectric constant has two factors: real ( $\epsilon_1$ ) and imaginary ( $\epsilon_2$ ) parts. Real and imaginary is correlated with this relation as  $(\omega) = \epsilon_1(\omega) + i\epsilon_2(\omega)$ . These parameters depend on ( $n$ ) and ( $k$ ) amounts, therefore are computed from these equations (Eq. 6) [55, 62]:

$$\begin{cases} \epsilon_1 = n^2 - k^2 \\ \epsilon_2 = 2nk \end{cases} \quad (6)$$

Where, ( $\epsilon_1$ ) and ( $\epsilon_2$ ) amounts depending on the wavelength,  $n$  and  $k$  parameters.

The real ( $\epsilon_1$ ) and imaginary ( $\epsilon_2$ ) merit is increased with increasing the wavelength and with doped nanomaterials of (Co<sub>3</sub>O<sub>4</sub>:Cr<sub>2</sub>O<sub>3</sub>) to the carbon as shown in Figures 11 and 12, that demonstrated the values of these parameters of the dielectric constant. The Figure 11 of the real part ( $\epsilon_1$ ) is related to the values of the refractive index ( $n$ ) and the extinction factor ( $k$ ) with equation 6. Therefore ( $n$ ) is higher than ( $k$ ) and the figure will be as the same shape of the refractive index ( $n$ ) [54, 62].

In Figure 12, the imaginary part ( $\epsilon_2$ ) of the dielectric constant related to the ( $n$ ) and ( $k$ ) also. But the value of ( $k$ ) is lower than ( $n$ ) and when multiplying ( $k$ ) by ( $n$ ), the result value is decreased from the product of multiplying, and the shape of a Figure 12 as the same figure of extinction coefficient for all thin films of the Nanocomposite.

### 3.1.7. Optical conductivity for the thin films

The optical conductivity ( $\sigma$ ) is depend on the absorbance coefficient ( $\alpha$ ) and the refractive index ( $n$ ). It is computed by utilizing this equation (Eq. 7) [63, 69]:

$$\sigma = \frac{\alpha n c}{4\pi} \quad (7)$$

Where, ( $\sigma$ ) is the optical conductivity ( $\Omega \cdot \text{cm}^{-1}$ ), ( $\alpha$ ) is the absorbance coefficient ( $\text{cm}^{-1}$ ), ( $n$ ) is the refractive index, and ( $c$ ) is the velocity of light ( $3 \times 10^{10}$  cm/s).

The variation of optical conductivity and the wavelength was shown in Figure 13. It is noticed, the optical conductivity value decreased at a wavelength ( $\lambda=370$  nm), and it becomes invariant along the wavelength axis as increases in doping with nanomaterials (Co<sub>3</sub>O<sub>4</sub>:Cr<sub>2</sub>O<sub>3</sub>) to carbon (C) for the concentration of samples (F, G, H, and I), but the optical conductivity of concentration for sample K (2.5:0.5/7 wt. %) is different from other concentrations,

its increased until a wavelength value ( $\lambda=370$  nm) and then be invariant along the wavelength axis. The concentration K is regarded as the best with high optical conductivity compare with other concentrations as shown in Figure 13.

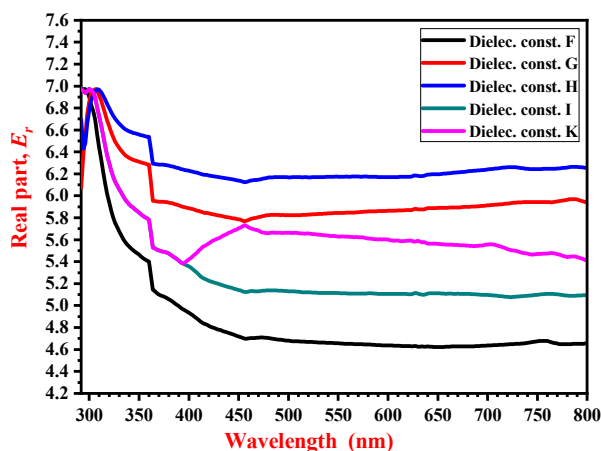


Figure 11: real part of dielectric constant with the wavelength for all thin films.

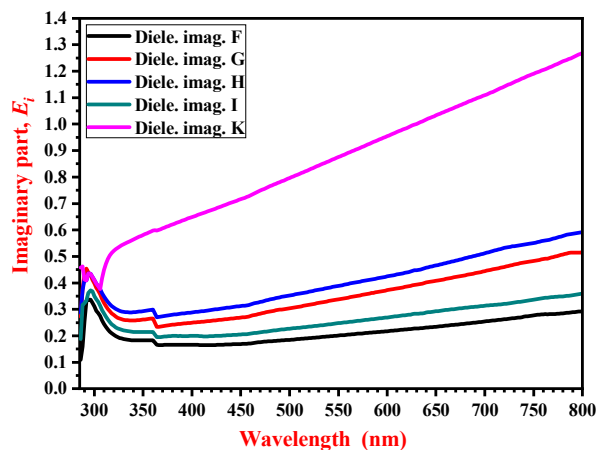


Figure 12: imaginary part of dielectric constant with the wavelength for all thin films.

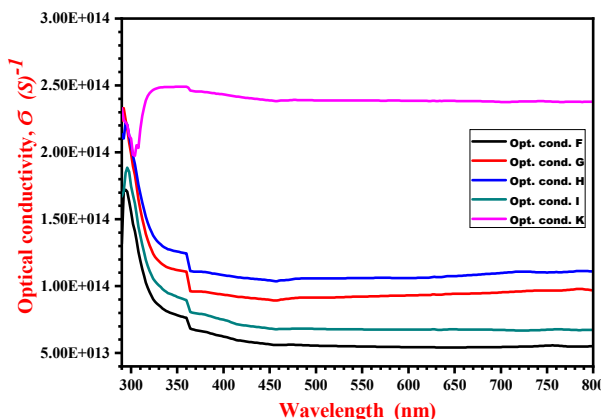


Figure 13: optical conductivity with the wavelength for all thin films.

### 3.1.8. Energy gap for the thin films

The band gap of the Nanocomposite thin films is defined by utilizing Tauc's relation and was depended on the absorption coefficient ( $\alpha$ ) and the photon energy ( $h\nu$ ) as shown in this equation (Eq. 8) [64, 70]:

$$\alpha h\nu = A (h\nu - E_g)^n \quad (8)$$

Where, ( $A$ ) is a constant, ( $E_g$ ) is the energy gap of the nanocomposite thin films, and ( $n$ ) is the power represents the value of the allowed transition ( $n = 0.5$  for indirect transition and  $n = 2$  for direct transition) [65, 66-70].

The nanocomposite thin films absorption of the wavelength for each concentration is depended on the confined region of the energy gap between the valence band and the conduction band, which accelerates the electrons between bands. Moreover, the high absorption energy of electrons in the nanocomposite thin films and will be through these band gaps, these values of energy gaps of the nanocomposite thin films, which is shown in Figure 14 very close to the energy gaps of the semiconducting materials.

Practically, to determine the energy gap of the nanocomposite thin films ( $\text{Co}_3\text{O}_4:\text{Cr}_2\text{O}_3/\text{C}$ ), by drawing the photon energy ( $h\nu$ ) versus  $(\alpha h\nu)^2$  and utilizing the information earned from the optical absorption spectra and was demonstrated in Figure 14 [55, 59-70].

In Figure 14 is exhibited the graph of energy gaps as a direct line in a definite region. Therefore, to gain the amount of direct allowed transition of the energy gap ( $E_g$ ) is depended on concentrations ( $\text{Co}_3\text{O}_4:\text{Cr}_2\text{O}_3$ ) to dope carbon (C) and creates thin films. By expanding the direct line and it is intercepted at ( $h\nu$ ) in the x-axis. It is noticed the optical energy gap was decreased with increasing the amount of nanomaterials ( $\text{Co}_3\text{O}_4:\text{Cr}_2\text{O}_3$ ) in nanocomposite thin films [7, 46]. The value of the energy gap ranging from (2.9-3.05 eV) is depended on the percentage of ( $\text{Co}_3\text{O}_4$ ) in samples, and its value in the ranging from (3.1 and 3.9 eV) depending on the content of ( $\text{Cr}_2\text{O}_3$ ) to dope carbon (C) in the samples, the interpreting is depending on the percentage of ( $\text{Co}_3\text{O}_4:\text{Cr}_2\text{O}_3$  to dope carbon, which is lead to this behavior [54, 58].

### 3.1.9. Urbach energy

In semiconductor materials, optical absorption spectra play an important part and provide the principal data the value of band gap. The optical absorbance spectra of the

semiconducting may be classified into two essential portions: (1) region of weakly absorbance, which can appear from impurities, defects, and the disorder of the lattice construction for the Nanocomposite, (2) vigorous absorbance which is determined from the optical energy gap. Urbach band tail is an exponential part that may be near the band gap edge and along with the absorbance coefficient curvature, the exponential band tail shows in a poor crystallinity, low crystallinity, these means the materials have an amorphous and disordered structure. Essential Urbach tail fall out in the lowest field of photon energy, because its depend on the absorbance coefficient ( $\alpha$ ) and photon energy ( $h\nu$ ), which is known by this equation (Eq. 9) [52, 54]:

$$\alpha = \alpha_o \exp \frac{h\nu}{E_u} \quad (9)$$

Where, ( $\alpha_o$ ) is a constant, and  $E_u$  is the Urbach energy.

By taking the logarithms for the two sides of the equation (9) and may give a straight-line equation (Eq. 10) and become as:

$$\ln \alpha = \ln \alpha_o + \frac{h\nu}{E_u} \quad (10)$$

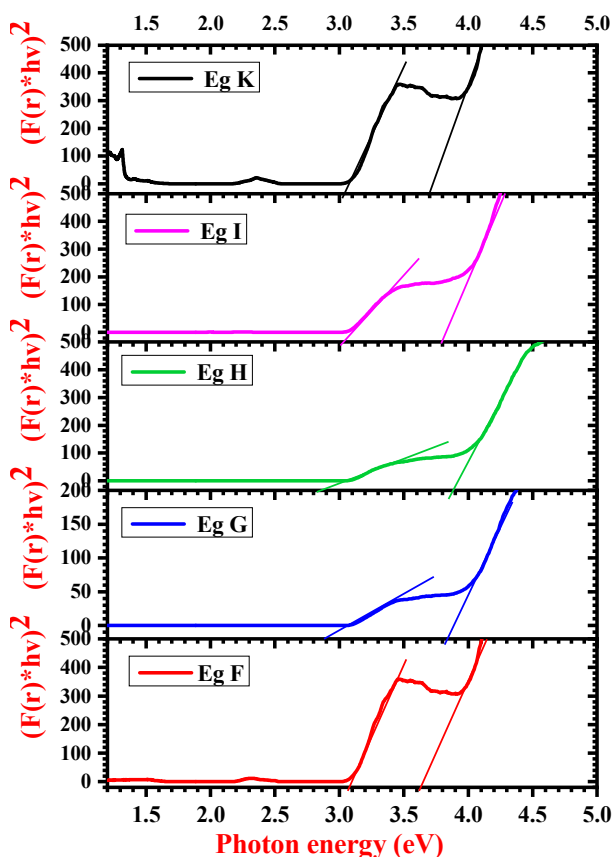


Figure 14: energy gap for all Nanocomposite thin films.

Theoretically, Urbach energy ( $E_U$ ) may be gained from the slope of the straight line by drawing  $\ln(\alpha)$  versus the photon energy ( $h\nu$ ). In Figure 15 shows the graphic presentation of  $\ln(\alpha)$  against ( $h\nu$ ). The slope for a straight line is equal to  $(1/E_U)$  and by intercepting y-axis in an amount is equal  $\ln(\alpha_0)$  for the nanocomposite thin films [54, 68].

It may be noticed, the amount of the Urbach energy ( $E_U$ ) is increased by increasing the rate of the (Co<sub>3</sub>O<sub>4</sub>:Cr<sub>2</sub>O<sub>3</sub>) amount in the nanocomposite thin films, but the correlation was exactly linear by taking the suitable fitting of all curves [50-70]. Further, it may notice from the Figure 15, the relation for the Urbach energy and the photon energy ( $h\nu$ ) will be fitted to gain a linear interrelation for all concentration of the Nanocomposite thin films. After then, the significant values for all specified parameters above are listed in Table 4.

#### 4. Absorptivity of samples

The absorptivity was calculated practically from the data for all samples around the solar energy radiation and is found the absorbance values are ranging between (88-93.2 %). These values of the absorptivity were coincided with the theoretical values that are gotten from the reflectivity test [67, 68]. Figure 16 is show the variation of the absorptivity with the temperatures for a long time during the day. The concentrations of all samples have high absorptivity compared with a one sample without coating.

In Figure 16, the absorbance is increased with temperatures; this depends on the morphology and roughness of the coated surfaces and its ability to absorb the solar energy radiation. The roughness of the coated surfaces prevents the reflection of solar energy

and the absorptivity increasing from the thin films coating on the surface [40-43].

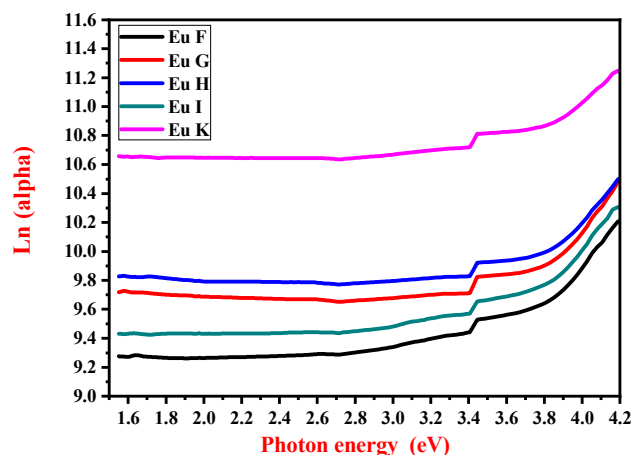


Figure 15: Urbach energy with photon energy for all samples.

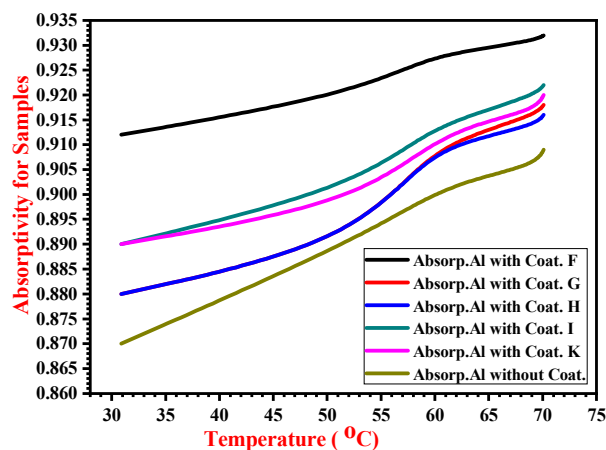


Figure 16: Absorptivity variation with the temperatures for all samples.

**Table 4:** the values of the absorbance edge, energy gap ( $E_g$ ), Urbach energy ( $E_U$ ), and ( $\alpha_0$ ) constant for the nanocomposite thin films.

Nanocomposite Thin films	Absorbance edge (nm)	Energy gap ( $E_g$ ) (nm)	Urbach energy ( $E_U$ ) (nm)	( $\alpha_0$ ) constant $\times 10^3$ (cm <sup>-1</sup> )
F	336	3.1, 3.6	13.57	9.338
G	336	2.9, 3.8	-41.81	17.668
H	342	2.9, 3.9	12.48	15.333
I	336	3.05, 3.8	5.12	8.343
K	368	3.05, 3.7	-12.25	52.152

## 5. Conclusion

Nanocomposite thin films ( $\text{Co}_3\text{O}_4:\text{Cr}_2\text{O}_3/\text{C}$ ) were synthesized for various concentrations ( $0.5:2.5 \leq x \leq 2.5:0.5$ ) wt. % of nanomaterials have been deposited on a preheated aluminum (Al) and glass substrates. Optical studies are revealed nanocomposite thin films have a good crystalline surface. The surface morphology has a roughness which is helped to absorb wavelength intensity. Optical properties were interpreted that, these nanocomposite thin films have been shifted for absorption edge at higher wavelengths when adding ( $\text{Co}_3\text{O}_4:\text{Cr}_2\text{O}_3$ ) to dope carbon (C). The thin films have high absorbance after doping, this is important to utilize this Nanocomposite as a coating on the flat plate collector to absorb the solar energy. So that the samples of the Nanocomposite were achieve a higher absorption coefficient ( $\alpha$ ). The skin depth ( $x$ ) and optical density ( $D_{opt.}$ ) have been computed and discussed also. Energy band gap results were calculated. The values are arranged about (2.9-3.9 eV). When carbon was doped with nanomaterials ( $\text{Co}_3\text{O}_4:\text{Cr}_2\text{O}_3$ ) which lead to a

decrease in energy gap values. The energy gap values are determined, which were good values compared with the other researchers. Urbach energy ( $E_u$ ) and its components were determined for the Nanocomposite; their values depend on the absorbance coefficient for Nanocomposite; these results were ascertained that these nanocomposite thin films are a semiconductor. The thin films's absorptivity values were determined between (88-93.2 %) and coincided with values computed from theoretical data obtained from reflectivity tests. The nanocomposites' applications are utilized as a coating on the flat plate collector and thermal concentrating system to absorb solar energy radiation for water heating in a domestic application.

## Acknowledgments

This work was supported by Al-Nahrain University from the Department of Chemistry, College of Science and Department of Mechanical Engineering, Engineering College.

## 6. References

1. K. T. Roro, N. Tile, B. Yalisi, M. De Gama, T. Wittes, T. Roberts, A. Forbes, Selective solar absorber coating research at the CSIR (South Africa), *world. Renew. energy Congr. /Sweden*, 61(2011), 4006-4013.
2. J. Moon, T. Kyoung Kim, B. Van Saders, C. Choi, Z. Liu, S. Jin, R. Chen, Black oxide nanoparticles as durable solar absorbing material for high-temperature concentrating solar power system, *Sol. Energy Mater. Sol. Cells*, 134(2015), 417– 424.
3. A. El-Aziz A. Said, M. M. Abd El-Wahab, S. A. Soliman, M. N. Goda, Synthesis and characterization of nano CuO-NiO mixed oxides, *Nanosci. Nanoeng.*, 1(2014), 17-28.
4. E. Yousif, M. Abdallah, H. Hashim, N. Salih, J. Salimon, B. Mudhaffar Abdullah, Yip-Foo Win, Optical properties of pure and modified poly (vinyl chloride), *Inter. J. Indus. Chem.*, 4(2013), 1-8.
5. M. Zahan, J. Podder, Surface morphology, optical properties and Urbach tail of spray deposited  $\text{Co}_3\text{O}_4$  thin films, *J. Mater. Sci.: Mater. in Electro.*, 30 (2019) 4259–4269.
6. H. Kim, D. W. Park, H. C. Woo, Chung, Environmental, Reduction of  $\text{SO}_2$  by C.O. to elemental sulfur over  $\text{Co}_3\text{O}_4\text{-TiO}_2$  catalysts, *Appl. Catal. B*, 19(1988), 233-243.
7. Cao, D., Chao, J., Sun, L., Wang, Catalytic behavior of  $\text{Co}_3\text{O}_4$  in electroreduction of  $\text{H}_2\text{O}_2$ , *J. Power Sources*, 179(2008), 87-91.
8. A. Szegedi, M. Popova, V. Mavrodinova, Minchevch, Cobalt-containing mesoporoussilicas-Preparation, characterization and catalytic activity in toluene hydrogenation, *Appl. Catal. A: Gen.l*, 338(2008), 44-51.
9. Logothesis, E. M., Park, K., Meitzler, A. H., Laud, K. R., Oxygen sensors using CoO ceramics, *Appl. Phys. Lett.*, 26(2008), 209-211.
10. M. M. Rahman, A. Jamal, S. Bahadar Khan, M. Faisal, Fabrication of highly sensitive ethanol chemical sensor based on Sm-Doped  $\text{Co}_3\text{O}_4$  nanokernels by a hydrothermal method, *J. Phys. Chem.*, 115(2011), 9503–9510.
11. S. Noguchi, M. Mizuhashi, Optical properties of Cr-Co oxide films obtained by chemical spray deposition: Substrate temperature effects, *Thin Solid Films*, 77(1981), 99-106.
12. D. Barreca, C. Massignan, S. Daolio, M. Fabrizio, C. Piccirillo, L. Armelao, E. Tondello, composition and microstructure of cobalt oxide thin films obtained from a novel cobalt (II) precursor by chemical vapor deposition, *Chem. Mater.*, 13(2001), 588-593.
13. C. S. Cheng, M. Serizawa, H. Sakata, T. Hirayama, Electrical conductivity of  $\text{Co}_3\text{O}_4$  films prepared by chemical vapor deposition, *Mater. Chem. and Phys.*, 53(1988), 225-230.
14. N. Kernavanois, E. Ressouche, P.J. Brown, J. Y. Henry, E. L. Berna, Magnetization distribution in

- paramagnetic CoO: a polarized neutron diffraction study, *J. Phys.: Condens. Matter*, 15(2003), 3433–3443.
15. X. He, X. Song, W. Qiao, Z. Li, X. Zhang, S. Yan, W. Zhong, Y. Du, Phase- and Size-Dependent Optical and Magnetic Properties of CoO Nanoparticles, *J. Phys. Chem.*, 17(2015), 9550-9559.
  16. Q. Tian, X. Wang, G. Huang, X. Guo, Nanostructured (Co, Mn)<sub>3</sub>O<sub>4</sub> for High Capacitive Supercapacitor Applications, *Nanoscale Res. Lett.*, 12(2017), 1-7.
  17. A. Hans, P. Garcia, Ronaldo, Jr. de Melo, A., C. B. Antonio, de Araujo, Optical and structural characterization of iron oxide and cobalt oxide thin films at 800 nm, *Appl. Phys. B*, 111 (2013), 313-321.
  18. J. Park, X. P. Shen, G. X. Wang, Solvothermal synthesis and gas-sensing performance of Co<sub>3</sub>O<sub>4</sub> hollow nanospheres, *Sens. Actuators B: chem.*, 136(2009), 494–498.
  19. Y. Wang, Z. Zhong, Y. Chen, C. T. Ng, J. Lin, Control able synthesis of Co<sub>3</sub>O<sub>4</sub> from nano size to micro size with largescale exposure of active crystal planes and their excellent rate capability in supercapacitors based on the crystal plane effect, *Nano Res.*, 4(2011), 695–704.
  20. D. Wang, X. Ma, Y. Wang, L. Wang, Z. Wang, W. Zheng, X. He, J. Li, Q. Peng, Y. Li, Shape control of CoO and LiCoO<sub>2</sub> Nanocrystals, *Nano Res.*, 3(2010), 1–7.
  21. S. N. Karthick, K. V. Hemalatha, C. Justin Raj, Hee Je Kim, Moonsuk Yi, Synthesis of nano-bound microsphere Co<sub>3</sub>O<sub>4</sub> by simple polymer-assisted sol-gel technique, *J. Nanoparticle Res.*, 15:1474(2013), 1-13.
  22. M. Salavati-Niasari, A. Khansari, F. Davar, Synthesis and characterization of cobalt oxide nanoparticles by thermal treatment process, *Inorganica Chim. Acta*, 362(2009), 4937–4942.
  23. Y. Qiang Mao, Z. Jiang Zhou, T. Ling and X. Wen Du, P-type CoO nanowire arrays and their application in quantum dot-sensitized solar cells, *RSC Adv.*, 3(2013), 1217-1221.
  24. R. Drasovean, S. Condurache Bota, Structural characterization and optical properties of Co<sub>3</sub>O<sub>4</sub> and CoO films, *J. Optoelectron. Adv. Mater.*, 11(2009), 2141–2144.
  25. F. I. Ezema, S. C. Ezugwu, S. N. Agbo, A. B. C. Ekwealor, P. U. Asogwa and R. U. Osuji, Synthesis and Characterization of Thallium Sulphide/Cadmium Sulphide and Lead Sulphide/Cadmium Sulphide Thin Films Grown in a Polymer Matrix by Chemical Bath Deposition (CBD) Method, 24th European Photovoltaic Solar Energy Conference, Hamburg, Germany, 295(2009), 295-298.
  26. Y. Liu, C. Wang, Y. Xue, The spectral properties and thermal stability of NbTiON solar selective absorbing coating, *Sol. Energy Mater. Sol. Cells*, 96(2012), 131–136.
  27. E. Echeverria, A. Kaphle, A. Austin, L. Bastatas, P. Hari, D. McIlroy, Evolution of the stoichiometry and electronic structure of cobalt oxide in thermally treated Co-Doped ZnO nanorods for solar cells, *ACS Appl. Nano Mater.*, 2(2019), 4113–4120.
  28. D. Liu, P. Yang, Controlling synthesis of metal organic framework derived Zn/Co/Ni oxide nanocomposites for applications, *J. Nanosci. Nanotechnol.*, 19(2019), 4414–4428.
  29. G. Li, M. Chen, Y. Ouyang, D. Yao, L. Lu, L. Wang, X. Xia, W. Lei, C. Shen-Ming, D. Mandle, Q. Hao, Manganese doped Co<sub>3</sub>O<sub>4</sub> mesoporous nanoneedle array for long cycle-stable supercapacitors, *Appl. Surf. Sci.*, 469(2019), 941-950.
  30. R. De1, S. Tripathi, S. C. Naidu, C. Prathap, J. Tripathi, J. Singh, S. Maidul Haque1, K. Divakar Rao1, N. K. Sahoo, Investigation on optical properties of spin coated TiO<sub>2</sub>/Co composite thin films, *AIP Conference Proceedings*, 1832(2017), 080038-1–080038-3.
  31. R. Perekrestov, A. Spesyvyi, J. Maixner, K. Mašek, O. Leiko, I. Khalakhan, J. Maňák, P. Kšírová, Z. Hubička, M. Čada, The comparative study of electrical, optical and catalytic properties of Co<sub>3</sub>O<sub>4</sub> thin nanocrystalline films prepared by reactive high-power impulse and radio frequency magnetron sputtering, *Thin Solid Films*, 686(2019), 137427-137461.
  32. M. Julkarnain, J. Hossain, K. Sharif, K. Khan, Optical properties of thermally evaporated Cr<sub>2</sub>O<sub>3</sub> thin film, *Can. J. Chem. Eng. Tech.*, 3(2012), 81–85.
  33. Y. Guo, S. J. Clark, J. Robertson, Electronic and magnetic properties of Ti<sub>2</sub>O<sub>3</sub>, Cr<sub>2</sub>O<sub>3</sub>, and Fe<sub>2</sub>O<sub>3</sub> calculated by the screened exchange hybrid density functional, *J. Phy. Conden. Matter*, 24(2012), 325504: 1-8.
  34. M. Palimi, M. Rostami, M. Mahdavian, B. Ramezan zadeh, Application of EIS and salt spray tests for investigation of the anticorrosion properties of polyurethane-based nanocomposites containing Cr<sub>2</sub>O<sub>3</sub> nanoparticles modified with 3-amino propyl trimethoxysilane, *Prog. Org. Coat.*, 77(2014), 1935–1945.
  35. S. W. Choi, A. Katoch, J. H. Kim, S. S. Kim, Prominent reducing gas-sensing performances of n-SnO<sub>2</sub> nanowires by local creation of p-n heterojunctions by functionalization with p-Cr<sub>2</sub>O<sub>3</sub> nanoparticles, *ACS Appl. Mater. Interfaces*, 6(2014), 17723–17729.
  36. S. Lei, X. Peng, Z. Liang, X. Li, C. Wang, B. Cheng, Y. Xiao, L. Zhou, Self-template formation and properties study of Cr<sub>2</sub>O<sub>3</sub> nanoparticle tubes, *J. Mater. Chem.*, 22(2012), 1643–1651.
  37. A. Kadari, T. Schemme, D. Kadri, J. Wollschläger, XPS and morphological properties of Cr<sub>2</sub>O<sub>3</sub> thin films grown by thermal evaporation method, *Results Phys.*, 7(2017), 3124-3129.
  38. K. AL-Rashedi, M. Farooqui and G. Rabba, Characterizing Crystalline Chromium Oxide Thin Film Growth by Sol-gel method on Glass Substrates, *Orient. J. Chem.*, 34(2018), 2203-2207.

39. M. M. Abdullah, F. M. Rajab, S. M. Al-Abbas, Structural and optical characterization of Cr<sub>2</sub>O<sub>3</sub> nanostructures: Evaluation of its dielectric properties, *AIP Adv.*, 4(2014), 027121-1-027121-11.
40. A. Gil, O. Kryshal, T. Brylewski, A. Czyska-Filemonowicz, Characterization of a Cr<sub>2</sub>O<sub>3</sub> scale formed on chromium with implanted yttrium ions by advanced electron microscopy, *Surf. Coat. Tech.*, 68(2019), 232-242.
41. S. Ponmudi, R. Sivakumar, C. Sanjeeviraja, C. Gopalakrishnan, K. Jeyadheepan, Tuning the morphology of Cr<sub>2</sub>O<sub>3</sub>:CuO (50:50) thin films by R.F. magnetron sputtering for room temperature sensing application, *Appl. Surf. Sci.*, 466(2019), 703-714.
42. L. Kotsedia, V. Furland, V. Bharadwaje, K. Kaviyarasua, B. Sotilloe, C.B. Mtshalia, N. Matinisea, A.G. Demird, B. Previtalid, R. Ramponie, S.M. Eatone, M. Maaza, Chromium oxide formation on nanosecond and femtosecond laser irradiated thin chromium films, *Opt. Mater.*, 95(2019), 109206-1-109206-7.
43. Z. Yuan, J. Zhao, F. Meng, W. Qin, Y. Chen, M. Yang, M. Ibrahim, Y. Zhao, Sandwich-like composites of double-layer Co<sub>3</sub>O<sub>4</sub> and reduced graphene oxide and their sensing properties to volatile organic compounds, *J. Alloys Compd.*, 793(2019), 24-30.
44. A. Hassena, S. El-Sayeda, W. M. Morsic, A. M. El Sayed, Preparation, Dielectric and optical properties of Cr<sub>2</sub>O<sub>3</sub>/PVC nanocomposite films, *J. Adv. Phys.*, 4(2014), 571-584.
45. A. B. Khelifa, A. Soum-Glaude, S. Khamlich, H. Glénat, M. Balgouthi, A. A. Guizani, M. Maaza, W. Dimassi, Optical simulation, characterization and thermal stability of Cr<sub>2</sub>O<sub>3</sub>/Cr/Cr<sub>2</sub>O<sub>3</sub> multilayer solar selective absorber coatings, *J. Alloys Compd.*, 783(2019), 533-544.
46. Z. Yang, W. Ren, L. Zhu, Y. Qing, Z. Huang, F. Luo, W. Zhou, Electromagnetic-wave absorption property of Cr<sub>2</sub>O<sub>3</sub>-TiO<sub>2</sub> coating with frequency selective surface, *J. Alloys Compd.*, 803(2019), 111-117.
47. N. Nasir, M. Kashif, N. Sabir, Z. Rizwan, Variation with Temperature in Photopyroelectric Spectroscopy and Electrical Parameters of ZnO + 1.0 MnO<sub>2</sub> + 0.8 Co<sub>3</sub>O<sub>4</sub> + xBi<sub>2</sub>O<sub>3</sub> + yTiO<sub>2</sub> Ceramics, *J. Nanomater. Bios.*, 14(2019), 61– 67.
48. M. V. Kanani, D. Dhruv, H. K. Rathod, K. N. Rathod, B. Rajyaguru, A. D. Joshi, P. S. Solanki, N. A. Shah, D. D. Pandey, Investigations on structural, optical and electrical property of ZnO-CuO core-shell nanocomposite, *Scr. Mater.*, 165(2019), 25–28.
49. C. M. Muiva, T. S. Sathiaraj, and J. M. Mwabora, Chemical bond approach to optical properties of some flash evaporated Se<sub>100-x</sub>Sb<sub>x</sub> chalcogenide alloys, *E.P. J. Appl. Phys.*, 59(2012), 1-7.
50. F. Cao, Ting Wang, Xiao hong J., Enhanced Visible Photocatalytic Activity of Tree-like ZnO/CuO Nanostructure on Cu Foam, *Appl. Surf. Sci.*, 471(2019), 417-424.
51. J. B. Chaudhari, N. G. Deshpande, Y. G. Gudage, A. Ghosh, V. B. Huse, Ramphal Sharma, Studies on growth and characterization of ternary CdS<sub>1-x</sub>Se<sub>x</sub> alloy thin films deposited by chemical bath deposition technique, *Appl. Surf. Sci.*, 254(2008), 6810–6816.
52. F. Urbach, The Long-Wavelength Edge of Photographic Sensitivity and of the Electronic Absorption of Solids, *Phys. Rev.*, 92(1953) 1324.
53. M. El-Hagary, M. E. Ismail, E. R. Shaaban, A. El-Taher, Effect of  $\gamma$ -irradiation exposure on optical properties of chalcogenide glasses Se<sub>70</sub>S<sub>30-x</sub>Sb<sub>x</sub> thin films, *Radiat. Phys. Chem.*, 81(2012), 1572-1577.
54. W. Al-Taa'y, M. A. Nabi, R. M. Yusop, E. Yousif, B. M. Abdullah, J. Salimon, N. Salih, S. I. Zubairi, Effect of Nano ZnO on the Optical Properties of Poly(vinyl chloride) films, *Int. J. Polym. Sci.*, Article ID 697809, vol. (2014), 1-6.
55. W. A. Al-Taa'y, A. A. Ameer, W. H. Al-Dahhan, M. Abdallh, E. Yousif, Optical constants of poly(vinyl chloride) doped by nano ZnO, *J. Chem. Pharm. Res.*, 7(2015), 536-541.
56. E. A. Sanchez-Ramirez, M. A. Hernandez-Perez, J. Aguilar-Hernandez, E. Rangel-Salinas, Nanocrystalline CdS<sub>1-x</sub>Se<sub>x</sub> alloys as thin films prepared by chemical bath deposition: Effect of x on the structural and optical properties, *J. Alloys Compd.*, 615(2014), S511-S514.
57. A. S. Hassanien, A. A. Akl, Influence of composition on optical and dispersion parameters of thermally evaporated non-crystalline Cd<sub>50</sub>S<sub>50-x</sub>Se<sub>x</sub> thin films, *J. Alloys Compd.*, 648(2015), 280-290.
58. W. A. Al-Taa'y, S. F. Oboudi, E. Yousif, M. A. Nabi, R. M. Yusop, D. Derawi, Fabrication and characterization of nickel chloride doped PMMA films, *Adv. Mater. Sci. Eng.*, Article ID 913260, vol. (2015), 1-5.
59. A. D. Achary, B. Sarwan, I. A. Malik, Y. A. Bhat, K. Silwa, M. K. Rathore, Optical Properties of NiO:PVA Thin Films, *AIP Conference Proceedings*, 2100 (2019), 1-5.
60. A. Kurt, Influence of AlCl<sub>3</sub> on the optical properties of new synthesized 3-armed poly(methyl methacrylate) films, *Turk. J. Chem.*, 34(2010), 67-79.
61. O. G. Abdullah, D. R. Saber, Optical absorption of poly-vinyl alcohol films doped with nickel chloride, *Appl. Mech. Mater.*, 110-116(2012), 177–182.
62. D.S. Ahmed, M. Abdallh, R. Alsayed, A. Ahmed, E. Yousif, Graft modification of PVC with 1,2,4-triazole ring system for preparing flexible PVC materials, *AIP Conference proceedings*, 2213, 020129 (2020).
63. J. Xiang, W. Lu, Y. Hu, Y. Wu, H. Yan, C.M. Lieber, Ge/Si nanowire heterostructures as high-performance field-effect transistors, *Nature*, 441(2006), 489-493.
64. W. A. Al-Taa'y, H. Ibraheem, E. Yousif, H. Jelassi, Studies on surface morphology and electrical conductivity of P.S. thin films in presence of divalent complexes, *Baghdad Sci. J.*, 16(2019), 588-594.
65. K.A. Aly, A. M. Abd Elnaeim, N. Afify, A.M. Abousehly, Improvement of the electrical properties

- of Se<sub>3</sub>Te<sub>1</sub> thin films by in additions, *J. Non Cryst. Solids*, 358(2012), 2759-2763.
66. A. A. Yadav, E. U. Masumdar, Preparation and characterization of indium doped CdS<sub>0.2</sub>Se<sub>0.8</sub> thin films by spray pyrolysis, *Mater. Res. Bull.*, 45(2010), 1455-1459.
67. R. N. Abed, Abdul Rahman N. Abed, F. A. Khamas, M. Abdallh, E. Yousif, Thermal coating comprising (CuO:NiO) nanocomposite/C Spectrally selective to absorb solar energy, *Prog. Color, Colorants, Coat.*, 13(2020), 275-284.
68. K. Zhang, K. Yu, Y. Liu, Y. Zhao, An improved algorithm for spectral emissivity measurements at low temperatures based on the multi-temperature calibration method, *Int. J. Heat Mass Transf.*, 114(2017), 1037–1044.
69. R. M. Omer, E. Yousif, E.T. B. Al-Tikrity, D. S. Ahmed, A. A. Ali, R. Abed, A detailed examination of U.V. radiation effects on the structural and morphological properties of polyvinyl butyral films containing different nanoparticles, *Prog. Color Colorants Coat.*, 14(2021), 209-219
70. R. N. Abed, M. Abdallh, A. A. Rashad, A. Hadawey, E. Yousif, New coating synthesis comprising CuO:NiO/C to obtain highly selective surface for enhancing solar energy absorption, *Polym. Bull.*, 78(2021), 433–455.

How to cite this article:

R. N. Abed, A. R. N. Abed, E. Yousif, Carbon Surfaces Doped with (Co<sub>3</sub>O<sub>4</sub>-Cr<sub>2</sub>O<sub>3</sub>) Nanocomposite for High-Temperature Photo Thermal Solar Energy Conversion Via Spectrally Selective Surfaces. *Prog. Color Colorants Coat.*, 14 (2021), 301-315.

